iScience

CellPress
OPEN ACCESS

Article

Urinary extracellular vesicles signature for diagnosis of kidney disease

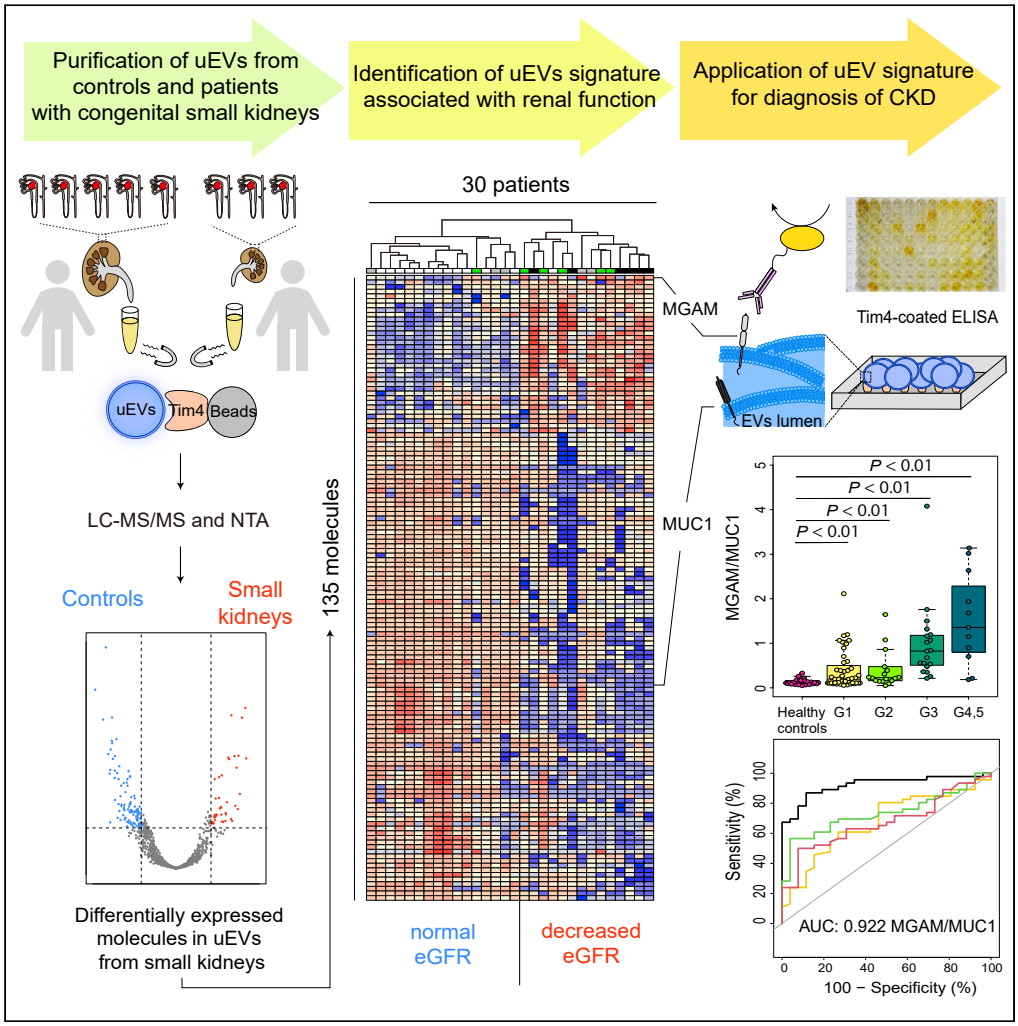

Keiichi Takizawa, Koji Ueda, Masahiro Sekiguchi, ..., Takanori Ichiki, Akira Oka, Yutaka Harita

haritay-ped@h.u-tokyo.ac.jp

Highlights

Urinary extracellular vesicles (uEVs) are altered in chronic kidney disease (CKD)

Characteristic expression signatures associated with childhood CKD are identified

An ELISA utilizing the signature detected decreased renal function

uEVs signature has potential in diagnosing kidney diseases

Takizawa et al., iScience 25, 105416
November 18, 2022
https://doi.org/10.1016/j.isci.2022.105416

iScience

CellPress
OPEN ACCESS

Article

Urinary extracellular vesicles signature for diagnosis of kidney disease

Keiichi Takizawa,[1] Koji Ueda,[2] Masahiro Sekiguchi,[1] Eiji Nakano,[1] Tatsuya Nishimura,[1] Yuko Kajiho,[1] Shoichiro Kanda,[1] Kenichiro Miura,[3] Motoshi Hattori,[3] Junya Hashimoto,[4] Yuko Hamasaki,[4] Masataka Hisano,[5] Tae Omori,[6] Takayuki Okamoto,[7] Hirotsugu Kitayama,[8] Naoya Fujita,[9] Hiromi Kuramochi,[10] Takanori Ichiki,[10] Akira Oka,[1] and Yutaka Harita[1,11,*]

SUMMARY

Congenital disorders characterized by the quantitative and qualitative reduction in the number of functional nephrons are the primary cause of chronic kidney disease (CKD) in children. We aimed to describe the alteration of urinary extracellular vesicles (uEVs) associated with decreased renal function during childhood. By nanoparticle tracking analysis and quantitative proteomics, we identified differentially expressed proteins in uEVs in bilateral renal hypoplasia, which is characterized by a congenitally reduced number of nephrons. This expression signature of uEVs reflected decreased renal function in CKD patients by congenital anomalies of the kidney and urinary tract or ciliopathy. As a proof-of-concept, we constructed a prototype ELISA system that enabled the isolation of uEVs and quantitation of expression of molecules representing the signature. The system identified decreased renal function even in its early stage. The uEVs signature could pave the way for non-invasive methods that can complement existing testing methods for diagnosing kidney diseases.

INTRODUCTION

Although diverse pathological conditions lead to chronic kidney disease (CKD) (Webster et al., 2017), irreversible loss of functional nephrons underlies its development and progression, irrespective of the cause (Fattah et al., 2019; Ruiz-Ortega et al., 2020). Recently, CKD in childhood has been the focus of research because it leads to substantial morbidity and mortality and also results in diverse medical issues beyond childhood (Ingelfinger et al., 2016; Stern-Zimmer et al., 2020). Unlike adult CKD, nonglomerular kidney diseases, including congenital anomalies of the kidney and urinary tract (CAKUT) and genetic disorders, account for most cases of CKD in children (Fathallah-Shaykh et al., 2015; Harambat et al., 2012). Early recognition in conjunction with a therapeutic intervention provides significant benefits for both childhood and adult CKD patients (Wühl et al., 2009). However, blood or urine tests may miss the early stages of nephron loss because of compensatory growth and hyperfunction of remaining nephrons (Fattah et al., 2019; Schnaper, 2014). Identifying novel urinary biomarkers that may predict disease progression has become an area of intense research (Good et al., 2010; Pontillo et al., 2017; Sandilands et al., 2013; Watson et al., 2019).

Extracellular vesicles (EVs) are particles naturally released from the cell delimited by a lipid bilayer and cannot replicate (Jeppesen et al., 2019; Théry et al., 2018; Tkach and Théry, 2016; van Niel et al., 2018). Urinary EVs (uEVs) or exosomes form a highly concentrated fraction containing cell-specific proteins from every nephron segment. uEVs can be a source of potentially valuable urinary biomarkers mirroring molecular processes in physiological and pathological conditions in the kidney and urinary tract (Erdbrügger et al., 2021; Pisitkun et al., 2004). uEV based search for biomarkers for various diseases, including acute kidney injury, glomerular diseases, renal tubular disorders, polycystic kidney disease, and transplanted kidneys, have been reported (Erdbrügger et al., 2021; Erdbrügger and Le, 2016).

This study aims to unravel the uEVs signature associated with CKD in childhood, which is less susceptible to acquired or secondary factors than kidney diseases in adults. These results offer proof of concept for the potential utility of altered uEVs signature in diagnosing childhood kidney diseases.

[1]Department of Pediatrics, Graduate School of Medicine, The University of Tokyo, 7-3-1 Hongo, Bunkyo-ku, Tokyo 113-8655, Japan

[2]Project for Personalized Cancer Medicine, Cancer Precision Medicine Center, Japanese Foundation for Cancer Research, Tokyo 135-8550, Japan

[3]Department of Pediatric Nephrology, Tokyo Women's Medical University, Tokyo 162-8666, Japan

[4]Department of Nephrology, Faculty of Medicine, Toho University, Tokyo 143-8541, Japan

[5]Department of Nephrology, Chiba Children's Hospital, Chiba 266-0007, Japan

[6]Department of Pediatrics, Tokyo Metropolitan Bokutoh Hospital, Tokyo 130-8575, Japan

[7]Department of Pediatrics, Hokkaido University Graduate School of Medicine, Hokkaido 060-8648, Japan

[8]Department of Nephrology, Shizuoka Children's Hospital, Shizuoka, 420-8660, Japan

[9]Department of Nephrology, Aichi Children's Health and Medical Center, Aichi 474-8710, Japan

[10]Department of Materials Engineering, School of Engineering, The University of Tokyo, Tokyo 113-8656, Japan

[11]Lead contact

*Correspondence: haritay-ped@h.u-tokyo.ac.jp

https://doi.org/10.1016/j.isci.2022.105416

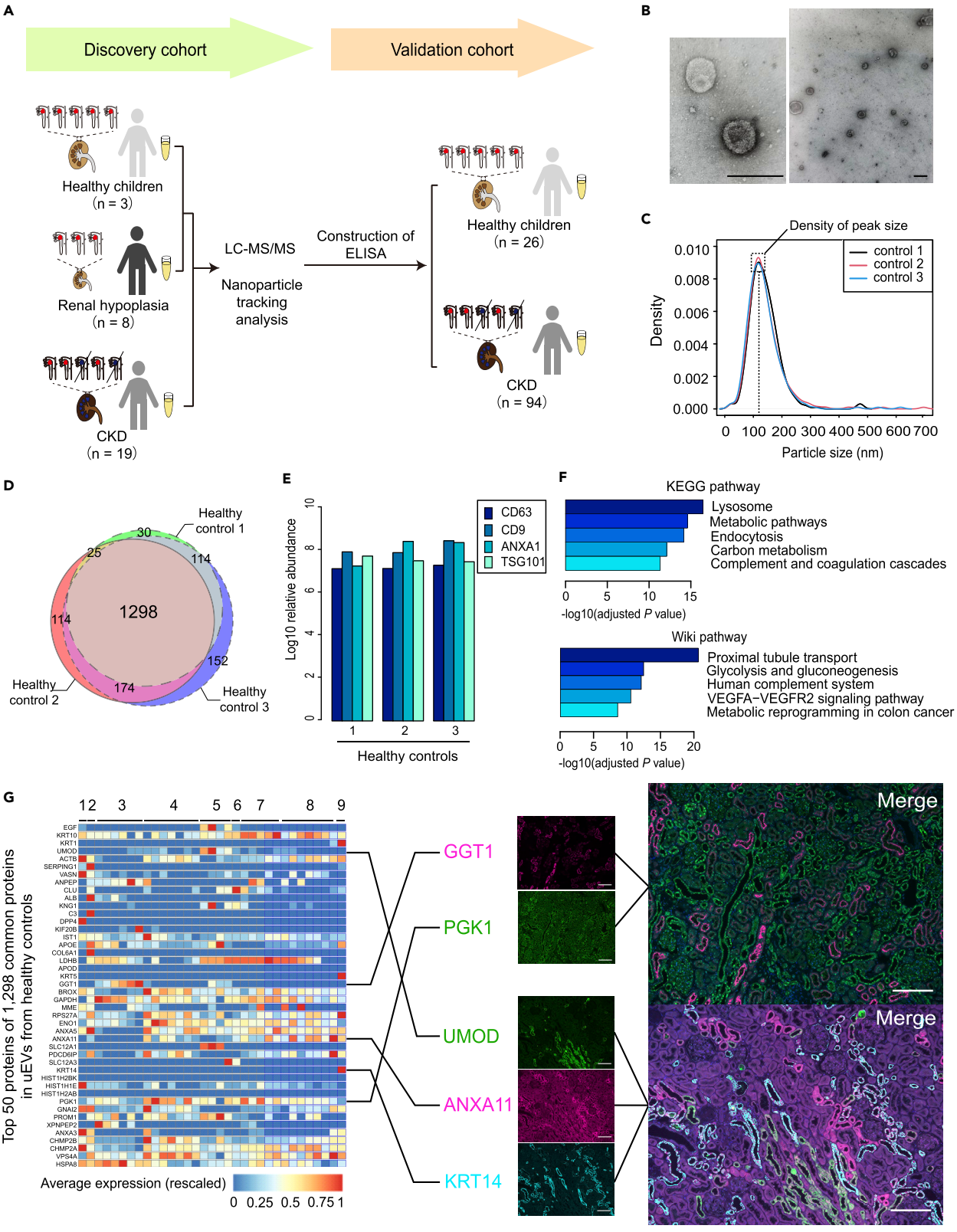
A
Discovery cohort
Validation cohort
Healthy children
(n = 3)
Renal hypoplasia
(n = 8)
CKD
(n = 19)
LC-MS/MS
Nanoparticle tracking analysis
Construction of ELISA
Healthy children
(n = 26)
CKD
(n = 94)
B
C
Density of peak size
control 1
control 2
control 3
Density
Particle size (nm)
D
Healthy control 1
Healthy control 2
Healthy control 3
1298
30
25
114
114
152
174
E
CD63
CD9
ANXA1
TSG101
Log10 relative abundance
Healthy controls
F
KEGG pathway
Lysosome
Metabolic pathways
Endocytosis
Carbon metabolism
Complement and coagulation cascades
-log10(adjusted P value)
Wiki pathway
Proximal tubule transport
Glycolysis and gluconeogenesis
Human complement system
VEGFA−VEGFR2 signaling pathway
Metabolic reprogramming in colon cancer
-log10(adjusted P value)
G
Top 50 proteins of 1,298 common proteins in uEVs from healthy controls
Average expression (rescaled)
GGT1
PGK1
UMOD
ANXA11
KRT14
Merge
Merge

Figure 1. Characterization of uEVs from healthy controls

(A) A schematic of the study outlining the discovery and validation cohort.

(B) Negative stain transmission electron microscopy of uEVs. Scale bars, 200 nm.

(C) Nanoparticle tracking analysis of uEVs isolated from healthy controls.

(D) Venn diagram of total proteins detected in uEVs isolated from healthy controls.

(E) Bar plot representing the abundance of common classical exosomal markers (CD63, CD9) and markers for classical microvesicles (Annexin A1) and arrestin-domain-containing protein 1-mediated microvesicles (TSG101) in healthy controls. The yaxis represents log10 relative abundance.

(F) KEGG/Wiki pathway analysis (g:profiler) of the 1,298 common proteins in uEVs from healthy controls. The top five terms with the lowest adjusted *p* values were extracted.

(G) Intrarenal expression of top 50 molecules in uEVs from healthy controls visualized using kidney cell explorer (Ransick et al., 2019) in order of relative abundance and immunofluorescence of human kidney specimens of 5 out of 50 molecules. Glutathione hydrolase 1 proenzyme (GGT1), phosphoglycerate kinase 1 (PGK1), uromodulin (UMOD), annexin A11 (ANXA11), keratin, and type I cytoskeletal 14 (KRT14) are expressed in the proximal tubule, loop of Henle, the distal tubule, collecting duct, and deep medullary epithelium of pelvis, respectively. The numbers above the figure represent each nephron segment: 1, podocytes; 2, parietal epithelium; 3, proximal tubule; 4, the loop of Henle; 5, distal tubule; 6, nephron connecting tubule; 7, cortical collecting duct; 8, medullary collecting duct; 9, deep medullary epithelium of pelvis. Scale bars, 200 μm.

RESULTS

Overview of human uEVs isolated using Tim4 beads

The study design is depicted in Figure 1A. Regarding the method to isolate uEVs, differential ultracentrifugation (Théry et al., 2018), the most commonly used technique, has several limitations (Dhondt et al., 2020; Merchant et al., 2017). It requires technical expertise that is prone to replication bias and can potentially damage EVs during the purification process (Dhondt et al., 2020). There are also problems with the affinity purification methods using exosome markers. The majority of uEVs do not express CD63 or CD9 (Blijdorp et al., 2021), suggesting that the methods using these molecules may lead to bias in the vesicles purified from urine. Here, we employed a Tim4-based purification system (Figure S1). The extracellular IgV-like domain of Tim4 binds phosphatidylserine on the surfaces of EVs, including exosomes and microvesicles (Nakai et al., 2016). Because the binding is Ca^{2+}-dependent, intact EVs can be easily released from Tim4-bound beads by adding Ca^{2+} chelators (Nakai et al., 2016). The morphology of uEVs purified from healthy controls by transmission electron microscopy matched with the typical saucer-like shape of EVs (Figure 1B) (Erdbrügger et al., 2021).

The number and size distribution of uEVs in the liquid suspension were analyzed by nanoparticle tracking analysis (NTA). The mean number (±SD) of uEVs isolated from three control samples was 19.19 (±7.19) $\times 10^9$ particles/mL. The mean size (±SD) of uEVs was 137.9 (±2.5) nm, with a peak at 117.4 nm (±1.0) (Figure 1C). The result was compatible with the size of uEVs in previous studies (Barreiro et al., 2020,2021).

The protein composition of uEVs isolated from control samples was analyzed using liquid chromatography-tandem mass spectrometry (LC-MS/MS). Subsequent Sequest database search identified 1,298 non-redundant proteins in all the three control samples (Figure 1D and Table S4). The list included most non-tissue-specific EV proteins (Category 1a) and cytosolic proteins recovered in EVs (Category 2) (Table S1) (Théry et al., 2018). As expected, common markers for exosome (CD63 and CD9), classical microvesicles (ANXA1), and arrestin domain-containing protein 1-mediated microvesicles (ARMM) (Tumor susceptibility gene 101 protein (TSG101)) (Jeppesen et al., 2019) were detected in all samples (Figure 1E). Kyoto Encyclopedia of Genes and Genomes (KEGG) and WikiPathways (Martens et al., 2021) analyses revealed several pathways enriched in the uEV proteome, including lysosomes, metabolic pathways, and endocytosis and proximal tubule transport (Figure 1F and Tables S5 and S6). Heterogeneity of cellular origins of purified vesicles was demonstrated by Kidney cell explorer (Ransick et al., 2019), which enables to visualize gene expression patterns across nephrons and ureteric epithelium cells, and also by immunofluorescence of human kidney specimens (Figure 1G).

Alteration of uEVs in renal hypoplasia

Next, we focused on uEVs isolated from patients with bilateral renal hypoplasia. Renal hypoplasia is characterized by congenitally small kidneys with fewer nephrons (Murugapoopathy and Gupta, 2020), and defined as a reduction of kidney size by two standard deviations from the mean size for the age (Rosenbaum et al., 1984). Renal scarring or renal atrophy secondary to acquired diseases was excluded. The patient characteristics are shown in Table 1. The protein composition of uEVs isolated from patients with renal hypoplasia was compared to that of uEVs isolated from the control samples after normalizing for the total protein in each uEV sample. Total protein amount is commonly used as a normalizing variable in calculating

Table 1. Baseline characteristics of participants in discovery cohort

Parameters	Healthy controls (n = 3)	Patients with renal hypoplasia (n = 8)	Other CKD patients (n = 19)
Age (year)	6.3 ± 2.5	9.5 ± 4.4	7.2 ± 4.5
Sex (male/female)	½	4/4	12/7
eGFR (mL/min/1.73m^2)	ND	29.4 ± 11.3	89.5 ± 35.9
Serum BUN (mg/L)	ND	45.1 ± 19.9	18.4 ± 11.4
Proteinuria (g/gCr)	ND	2.49 ± 4.49	0.22 ± 0.39
Urine creatinine (mg/dL)	84.8 ± 44.1	41.7 ± 21.8	59.7 ± 38.2

Plus-minus values are the mean ± SD.
ND, not done.

relative excretion rate for EVs (Erdbrügger et al., 2021; Théry et al., 2018). The uEVs from all the patients with renal hypoplasia contained marker proteins for classical exosomes (CD63 and CD9), classical microvesicles (ANXA1), and ARMM (TSG101) (Figure 2A). We applied differential enrichment analysis by protein-wise linear models combined with empirical Bayesian statistics to identify the proteins that best-distinguished samples from patients with renal hypoplasia and healthy controls. It revealed a total of 135 discriminatory proteins, among which 35 and 100 proteins were increased and decreased, respectively, in renal hypoplasia (Figure 2B and Table S7). Multidimensional scaling (MDS) analysis using the expression levels of these 135 proteins in uEVs distinguished healthy controls from patients with renal hypoplasia (Figure 2C). Gene ontology analysis revealed that proteins upregulated in renal hypoplasia are associated with immune-mediated pathways (Figure 2D), suggesting possible chronic inflammation in the kidneys of patients with CKD (Akchurin and Kaskel, 2015). On the contrary, proteins with decreased levels in renal hypoplasia were associated with electrolyte transfer in the tubules, such as in chloride ion homeostasis and monovalent inorganic anion homeostasis (Figure 2D). These molecules were not expressed exclusively in any nephron segments (Figures 2E and 2F).

The expression signatures and characteristics of uEVs in CKD patients

Next, we analyzed samples from patients with CKD presenting with various kidney functions by congenital anomalies of the kidney and urinary tract (vesicoureteral reflux, solitary kidney, or unilateral renal hypoplasia with compensatory contralateral renal hypertrophy) or ciliopathies (nephronophthisis or polycystic kidney) (Table 1). These data were combined with the data of uEVs from control and bilateral renal hypoplasia. Unsupervised consensus clustering of 30 uEVs samples was performed using quantitative expression data for 135 proteins distinguishing bilateral renal hypoplasia from control (Figure 2B). It revealed that these uEVs samples were classified into two major clusters (Cluster 1 and 2) (Figure 3A). The mean eGFR of patients in Cluster 1 was 99.2 mL/min/1.73m^2, and that in Cluster 2 was significantly decreased, being 46.0 mL/min/1.73m^2 (Table S2). The abundance of representative proteins assessed by LC-MS/MS analysis in patients with eGFR 90 mL/min/1.73m^2 or higher (N) and those with eGFR lower than 90 mL/min/1.73m^2 (D) is shown in Figure 3B. MDS analysis using quantitative proteome data demonstrated that the uEV proteome could distinguish patients with decreased renal function (Figure 3C). The results suggested that the expression of these proteins could potentially be used for screening urine from patients with decreased renal function.

The characteristics of uEVs in CKD patients

Next, we examined whether the physical characteristics of uEVs is altered in CKD. NTA was performed on 20 samples that were available in the quantity required for the study. As previously reported (Blijdorp et al., 2021), the number of particles is positively correlated with urine creatinine (Figure 4A), and both are negatively correlated with the mean size of uEVs (Figures 4B and 4C). Although the number of particles and mean size of uEVs from patients with CKD and controls was not statistically different, the relative density of peak size was significantly lower in patients with CKD than in controls ($p = 0.007$) (Figures 4D–4G).

We examined whether the morphology of uEVs is altered by urine creatinine. In samples with low urine creatinine (uCr: <50 mg/dL), the ratio of larger vesicles (150-1000 nm) was more prominent than those with high creatinine (uCr: ≥50 mg/dL) (Figure S2).

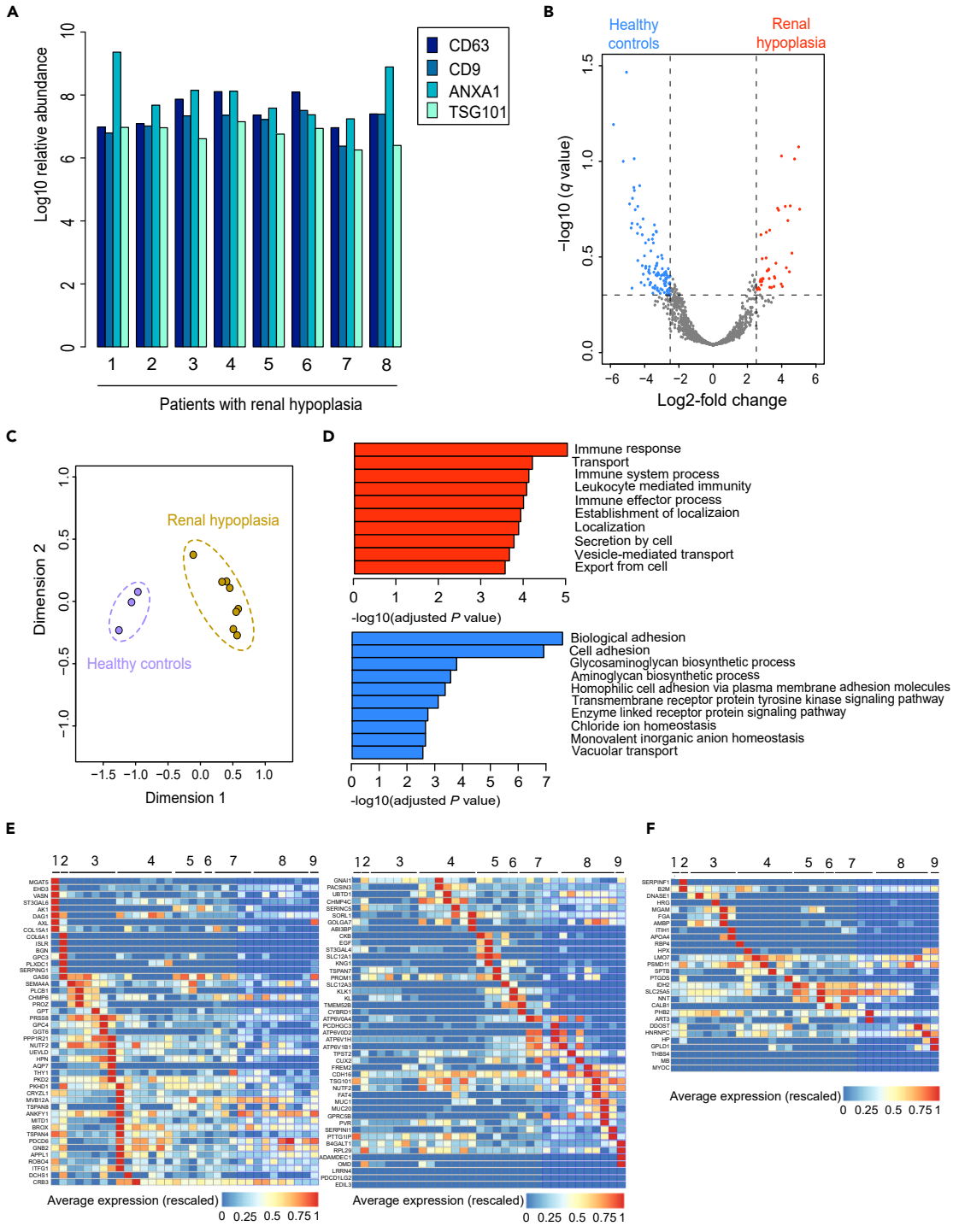

Figure 2. Alteration of uEVs in renal hypoplasia

(A) Bar plot representing the abundance of common classical exosomal markers (CD63, CD9) and markers for classical microvesicles (Annexin A1) and arrestin-domain-containing protein 1-mediated microvesicles (TSG101) in patients with renal hypoplasia. The yaxis represents log10 relative abundance.

(B) Volcano plot displaying uEV proteins that are differentially expressed between healthy controls and patients with renal hypoplasia. One hundred proteins highly expressed in healthy children are shown in blue, and 35 proteins highly expressed in patients with renal hypoplasia are shown in red.

(C) Multidimensional scaling (MDS) analysis based on quantitative profiles of 135 differentially expressed proteins.

Figure 2. *Continued*

(D) Biological process by gene ontology (GO) analysis (g:profiler) of 35 upregulated (red) and 100 downregulated (blue) proteins in uEVs from patients with renal hypoplasia.

(E and F) Expression of the downregulated (E) and upregulated (F) molecules in the kidney as visualized using kidney cell explorer. The numbers above the figure are the same as in Figure 1G.

Construction of an ELISA platform for the detection of uEVs signature

For proof of concept that the uEVs signature is associated with CKD, we aimed to establish an ELISA platform using Tim4 as an EV-capture substance and biotinylated antibodies as detection antibodies (Figures 5A andS3). The system quantifies the protein content of candidate biomarkers in uEVs in simple steps. Among the molecules commonly increased in uEVs in bilateral renal hypoplasia or CKD, MGAM was the only transmembrane protein for which antibodies to the extracellular region were available (Figure 3B). To narrow the list of molecules that are decreased in CKD, we used the following criteria: a membrane protein that is localized on the cell surface of renal cells, for which antibodies against the extracellular region are available, and whose signal is stably detected in the proteome of normal urine. Five molecules (MUC1, PVR, PKD2, PROM1, and THY1) met the criteria (Figure 3B). Finally, we examined whether commercially available antibodies can be used to evaluate their expression in Tim4-purified uEVs. Through this analysis, we finally succeeded in constructing a quantitative system for MUC1 and MGAM (Figures S3 and S4). MUC1 is a transmembrane glycoprotein, the expression of which is limited to the apical surface of distal convoluted tubules and collecting ducts. MGAM, an alpha-glucosidase, is exclusively expressed in proximal tubular cells in the kidney (Figure 5B). In addition, because the size of decreased particles in patients with CKD corresponds to the size of the classical or nonclassical exosome (Figure 4D) (Jeppesen et al., 2019), we also included CD9 and CD63 as markers for these small EVs (Figure S4) (Jeppesen et al., 2019). CD9 is expressed along the basal membrane of the distal convoluted tubule and the collecting duct (Figure 5B) (Blijdorp et al., 2021).

We examined whether the number of freeze-thaw cycles of urine samples and the presence or absence of protease inhibitors affects these assays' results. As shown in Figures S5A–S5D, the number of freeze-thaw cycles up to three or the absence of protease inhibitors did not affect the results. We also analyzed whether the vesicles are stable for prolonged periods in urine. One month of frozen urine storage did not interfere with the detection of CD9, indicating that uEVs is stable in frozen urine (Figure S5E).

The utility of uEVs for detection of CKD

We examined MUC1 concentrations by ELISA using discovery cohort. The sample size required for identification of decreased renal function eGFR <60 or <90 by MUC1 was calculated as 10.8 or 23.9, respectively.

We collected urine samples from 26 controls and 94 pediatric patients with CKD (validation cohort; Table 2). Reflecting the etiology of childhood CKD (Harada et al., 2022), patients suffer mainly CAKUT, and none have diabetes or diabetic kidney disease. We quantified MUC1, MGAM, CD9, and CD63 levels in uEVs by ELISA (Figures 6A and S6). The expression levels of MUC1, MGAM, CD9, and CD63 in uEVs did not correlate with the urine albumin (Figure S7). Noticeably, the expression level of CD9 is highly correlated with that of MUC1 in both discovery and validation cohorts (Figure S8), and they were significantly decreased in CKD (Figures 6A and S6).

Receiver operating characteristic (ROC) curve analysis was performed to assess the discriminatory performance in identifying patients with decreased renal function. The univariate analysis using MUC1 level in uEVs showed high diagnostic performance for discriminating patients with eGFR<60 (Figure 6B) or <90 mL/min/1.73m^2 (Figure 6C). The AUC values increased further in bivariate analysis with MUC1 and MGAM. In the tri-variate analysis using MUC1, MGAM and CD9, achieved the highest AUC values of 1.000 (eGFR<60) (Figures 6B) and 0.953 (eGFR<90) (Figure 6C). We also examined whether this method could differentiate patients with CKD having normal eGFR (eGFR $\geq$90) from healthy controls. AUC values of bivariate or tri-variate analysis exceeded 0.75 (Figure 6D), suggesting that uEVs signature may detect changes in kidneys even in CKD patients with normal eGFR.

We also investigated whether the expression value of MGAM divided by that of MUC1 (MGAM/MUC1), instead of a combined multivariate analysis, could be used as an index for declined renal function. The

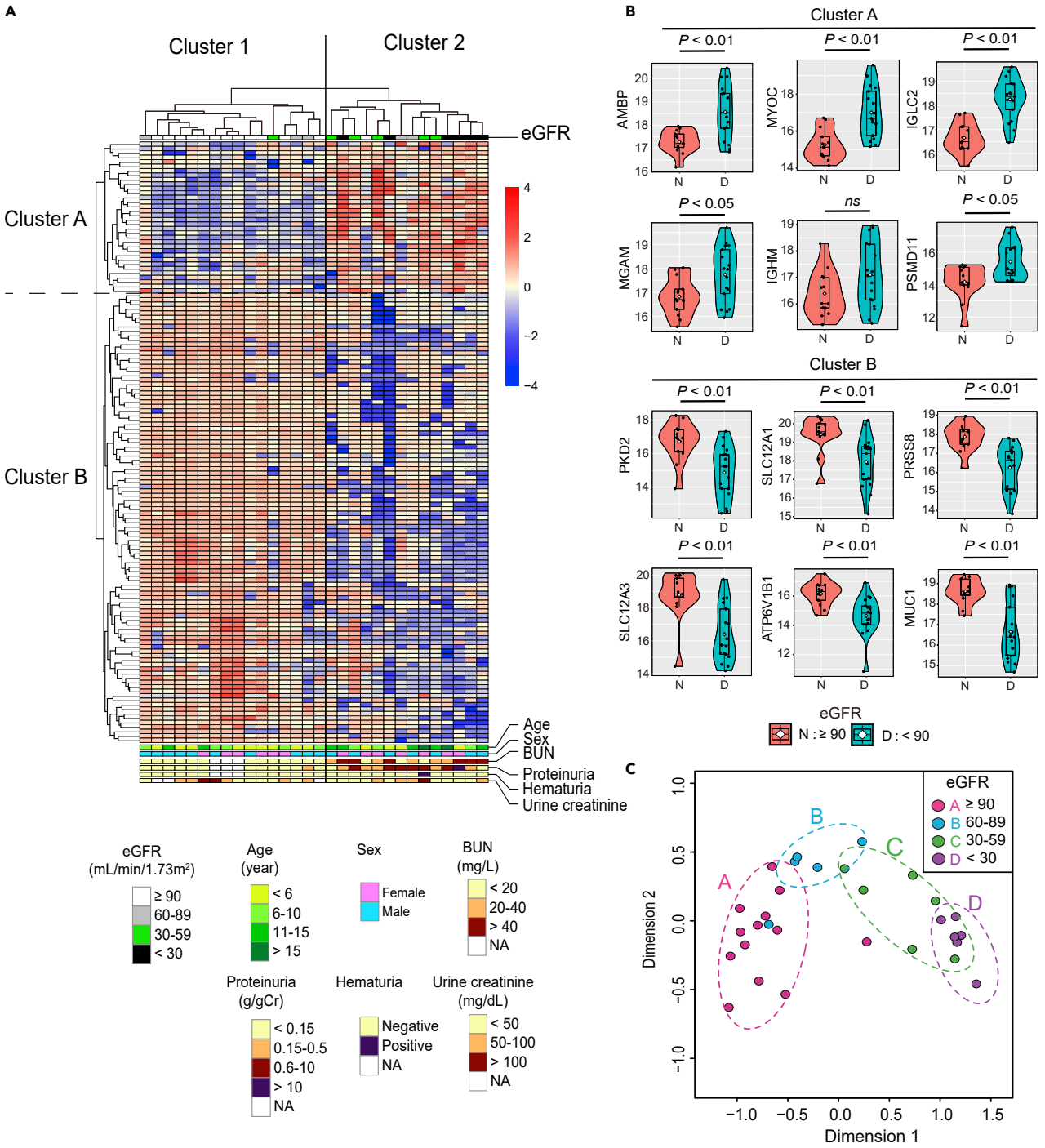

Figure 3. Altered uEVs signature in CKD

(A) Heatmap of the expression of 135 proteins and clinical information of 30 patients. The expression level was log-transformed and z-normalized to zero mean and unit standard deviation for each protein.

(B) Violin plot showing the examples of expression of proteins in uEVs from individuals with normal renal function (N: eGFR ≥90 mL/min/1.73m^2) or patients with decreased renal function (D: eGFR <90 mL/min/1.73m^2). Data were compared using the two-tailed Mann–Whitney *U* test. *ns* = not significant.

(C) MDS analysis based on quantitative profiles of 135 differentially expressed proteins.

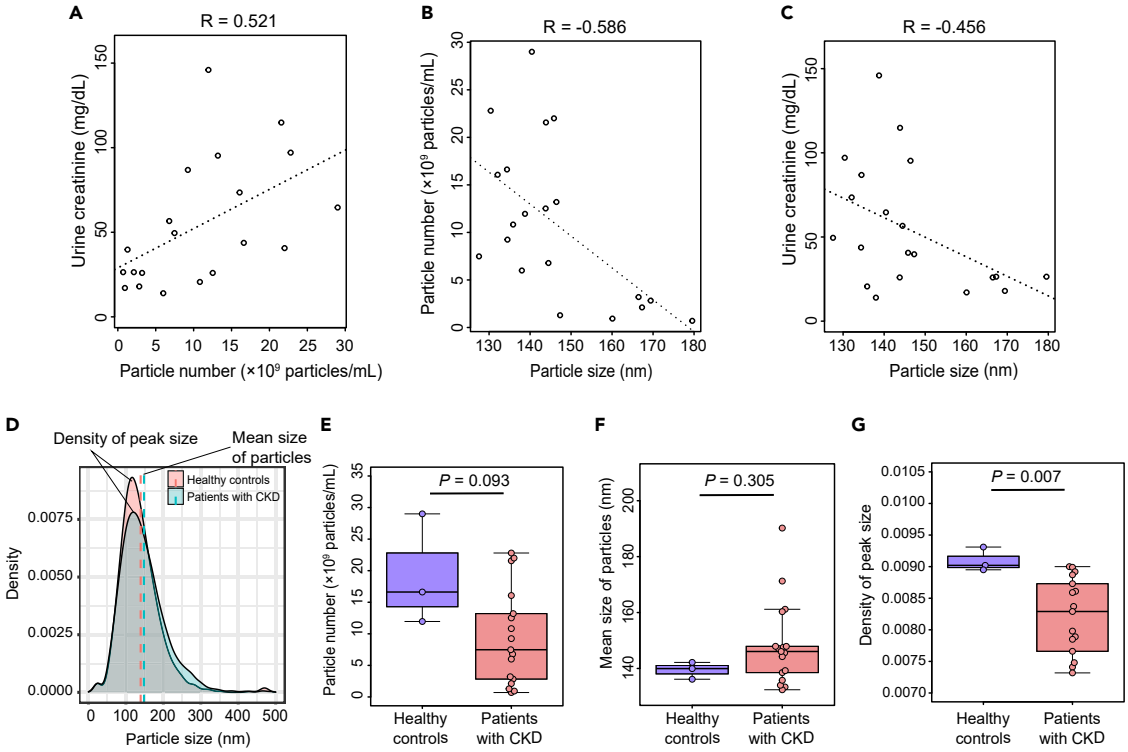

Figure 4. Morphological characteristics of uEVs in CKD

(A–C) Correlation plot of particle number and urine creatinine (A), of particle size and particle number (B), and of particle size and urine creatinine (C). Correlation coefficients are expressed as Pearson's R.

(D) Density plot showing the size distribution of particles in healthy controls and patients with CKD. The dotted line shows the mean size of particles in each group.

(E–G) Boxplots comparing particle number (E), mean size of particles (F) and density of peak size (G) between samples of healthy controls and patients with CKD. Boxes in boxplots indicate the 25th and 75th percentiles, and the horizontal lines inside the boxes indicate the median. Bars indicate the 10th and 90th percentiles. Data were compared using the two-tailed Welch's *t* test.

See also Figure S2.

MGAM/MUC1 value increased as renal function decreased in the discovery and validation cohorts (Figure 6E). The MGAM/MUC1 value yielded an AUC of 0.922 for separating patients with decreased renal function (eGFR <90) (Figure 6F). The sensitivity and specificity of MGAM/MUC1 for the diagnosis of decreased eGFR were 88.5 and 87.5%, respectively, based on the ROC curve-derived optimal cutoff value. It achieves significantly higher accuracy than urine creatinine, albumin, or L-FABP, suggesting that the new method captures changes that existing urine biomarkers cannot detect (Figure 6F).

Finally, we analyzed the association between MGAM/MUC1 and renal prognosis. Among the patients in the discovery and validation cohorts, follow-up data more than six months after the initial analysis were available on 35 patients (Table S3). According to the MGAM/MUC1 values in the initial analysis, these patients were classified into two groups. The threshold (0.35) was set to include the maximum value (0.330) of the healthy control's MGAM/MUC1 value. The mean period from the initial analysis to the follow-up analysis was 25.8 (±14.4) months. In patients with MGAM/MUC1 less than 0.35 (<0.35; 6 patients), the mean eGFR at onset was 86.7 (±26.7) mL/min/1.73m^2. In this group, eGFR did not change significantly during the follow-up period. The mean eGFR at onset of the patients with MGAM/MUC1 above 0.35 (≥0.35; 29 patients) was lower than MGAM/MUC1 < 0.35 group (65.4 ± 36.2 mL/min/1.73m^2), and some experienced a significant further decline in eGFR (Figure 6G).

Recently it has been reported that adult women excrete fewer uEVs than men (Blijdorp et al., 2022). We performed separate analyses for male and female controls or patients in validation cohort. A gender effect was not clearly demonstrated in this study (Figures S9 and S10).

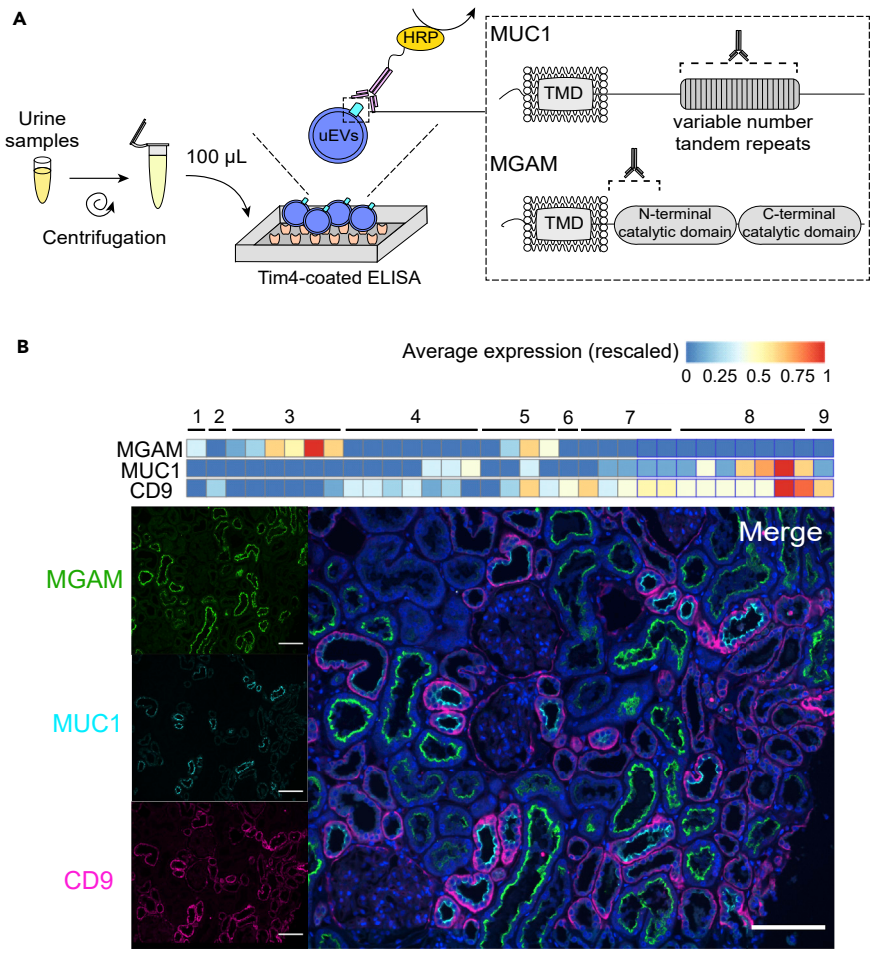

Figure 5. ELISA platform for assessment of uEVs

(A) Schematic illustration of sandwich ELISA using Tim4.

(B) Expression of MGAM, MUC1, and CD9 in nephron segments. The expression pattern was visualized by kidney cell explorer and by fluorescent immunohistochemistry using human kidney tissue. The numbers above the figure are the same as in Figure 1G. Scale bars, 100 µm.

See also Figures S4 and S5.

Urinary concentrations of MUC1 have been reported to be potentially associated with renal disease. Patients with hypercalciuric nephrolithiasis had significantly decreased levels of urinary MUC1 (Nie et al., 2016). Furthermore, urinary MUC1 fragment that is shed from renal tubular epithelium is reported as a biomarker associated with renal dysfunction (Zhang et al., 2017). We examined the correlation between the concentration of MUC1 in urine and in uEVs. As shown in Figure S11, no correlation between these two values was found. This result suggested that the change in MUC1 in uEVs captures factors in kidney tissue, independent of the urinary concentration of soluble MUC1 fragment.

DISCUSSION

In diagnosing kidney disease, urine tests for hematuria or proteinuria are crucial. However, conventional urine tests may miss certain forms of diseases which do not accompany hematuria or proteinuria or reduce the ability to concentrate urine. Here, we examined the usefulness of uEVs for CKD diagnosis. The affinity method using Tim4-coupled beads (Figure S1) allows for the rapid and simple purification of uEVs, ensuring their diversity (Figure 1). This method is suitable for analyzing samples with diverse clinical backgrounds.

The proteomic analysis identified a list of proteins, the contents of which in uEVs were distinctly altered in patients with bilateral renal hypoplasia (Figure 2 and Table S7). This uEV signature helped distinguish CKD

Table 2. Characteristics of 120 participants in validation cohort

Parameters	CKD patients (n = 94)	Healthy controls (n = 26)
Age (year)	7.8 ± 6.1	5.1 ± 3.6
Gender n (%)		
Female	27 (29)	13 (50)
Male	67 (71)	13 (50)
Disease n (%)		
Renal hypoplasia	26 (27.7)	NA
Ciliopathy	5 (5.3)	
Polycystic kidney disease	4 (4.3)	
Multicystic dysplastic kidney	9 (9.6)	
Solitary kidney	8 (8.5)	
Vesicoureteral reflux	12 (12.8)	
Hydronephrosis	9 (9.6)	
Others[a]	21 (22.3)	
Examination results		
eGFR (mL/min/1.73m^2)	80.6 ± 39.6	ND
Serum BUN (mg/L)	21.4 ± 17.9	
Proteinuria (g/gCr)	0.57 ± 1.35	

Plus-minus values are the mean ± SD.

NA, not applicable; ND, not done.

[a]Horseshoe kidney, renal tubular dysgenesis, posterior urethral valve, ureteral aneurysm, henoch-schönlein purpura nephritis, nephrotic syndrome, asymptomatic proteinuria, obesity-related glomerulopathy, Epstein syndrome, nephrogenic diabetes insipidus, chronic kidney disease because of DOHaD, megaloureter, dysplastic kidney, nephrocalcinosis, renal injury due to severe neonatal asphyxia.

patients with a decreased renal function (Figure 3). To validate the changes in uEVs expression pattern in CKD, we performed an independent validation study on samples from patients with diverse renal functions using an ELISA-based quantification system, which quantifies the expression levels of several proteins on the membrane surface of uEVs (Figures 5 and 6). The prototype discriminated CKD in its early stage or even with normal kidney function (Figure 6).

Distal tubule/collecting duct-specific MUC1 was among the molecules decreased in uEVs in renal hypodysplasia. MUC1 has numerous functions in the normal and injured kidney. Mutations in the *MUC1* gene cause slowly progressive tubulointerstitial disease that leads to kidney failure (Dvela-Levitt et al., 2019; Kirby et al., 2013), and aberrant activation of MUC1 signaling is associated with the development of CKD (Al-Bataineh et al., 2017). Decreased expression of MUC1 in uEVs implies decreased excretion of classical exosome because of functional nephron loss. Indeed, we do show that (1) the cells expressing MUC1 is largely overlapped with those expressing CD9 (Figure 5B) (2) The expression levels of MUC1 and CD9 in uEVs were highly correlated (Figure S8) and significantly decreased in CKD (Figures 6A and S6). This is in agreement with previous work showing the alteration of the expressional pattern of CD9 in uEVs by chronic nephron loss. Salih et al. found that abundance of CD9 was significantly reduced in patients with progressive autosomal dominant polycystic kidney disease (Salih et al., 2016). Recently, Blijdorp et al. demonstrated that donor nephrectomy reduced eGFR and CD9$^+$ uEVs (presumably derived from distal nephron), whereas the excretion of CD9$^-$uEVs was not altered (Blijdorp et al., 2022).

Another example of EV signature is proximal tubule-specific MGAM, which was increased in uEVs in renal hypodysplasia. Although the validation cohort did not show a statistically predominant increase of MGAM in CKD (Figure 6A), it is thought to capture different aspect of uEVs from decreased MUC1 expression as it improves diagnostic ability when combined with MUC1 (Figures 6B–6D). MGAM was previously reported to be the top discriminating protein for acute kidney injury in patients with cirrhosis (Awdishu et al., 2019). The present results suggest that MGAM is also involved in changes in the chronic phase. The relative increase in

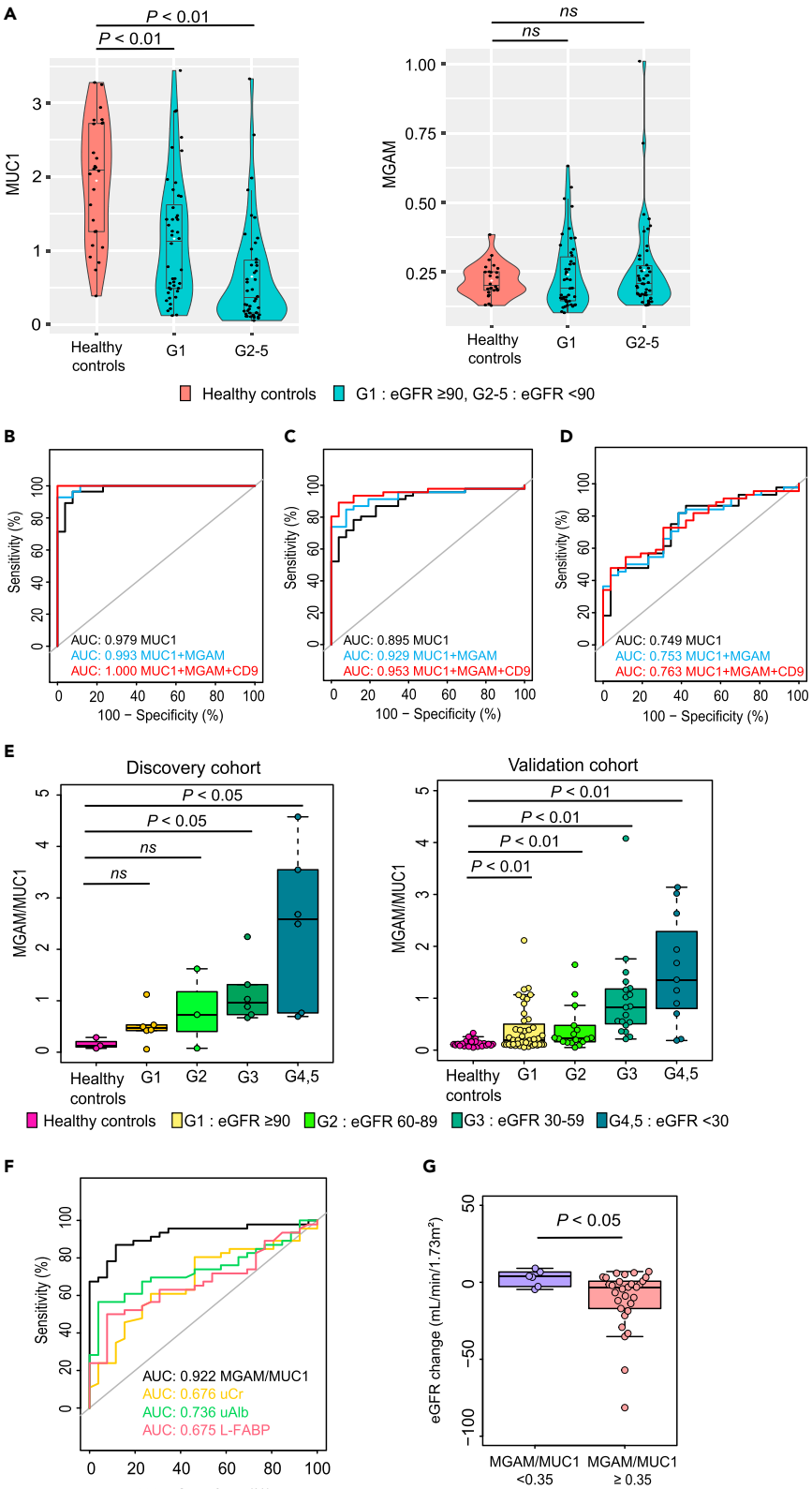
A
P < 0.01
P < 0.01
MUC1
Healthy controls
G1
G2-5
ns
ns
MGAM
Healthy controls
G1
G2-5
Healthy controls
G1 : eGFR ≥90, G2-5 : eGFR <90
B
Sensitivity (%)
AUC: 0.979 MUC1
AUC: 0.993 MUC1+MGAM
AUC: 1.000 MUC1+MGAM+CD9
100 − Specificity (%)
C
Sensitivity (%)
AUC: 0.895 MUC1
AUC: 0.929 MUC1+MGAM
AUC: 0.953 MUC1+MGAM+CD9
100 − Specificity (%)
D
Sensitivity (%)
AUC: 0.749 MUC1
AUC: 0.753 MUC1+MGAM
AUC: 0.763 MUC1+MGAM+CD9
100 − Specificity (%)
E
Discovery cohort
P < 0.05
P < 0.05
ns
ns
MGAM/MUC1
Healthy controls
G1
G2
G3
G4,5
Validation cohort
P < 0.01
P < 0.01
P < 0.01
P < 0.01
MGAM/MUC1
Healthy controls
G1
G2
G3
G4,5
Healthy controls
G1 : eGFR ≥90
G2 : eGFR 60-89
G3 : eGFR 30-59
G4,5 : eGFR <30
F
Sensitivity (%)
AUC: 0.922 MGAM/MUC1
AUC: 0.676 uCr
AUC: 0.736 uAlb
AUC: 0.675 L-FABP
100 − Specificity (%)
G
P < 0.05
eGFR change (mL/min/1.73m²)
MGAM/MUC1 <0.35
MGAM/MUC1 ≥ 0.35

Figure 6. Application of expression signature of uEVs for diagnosis of CKD

(A) Comparison of MUC1 and MGAM levels (absorbance at 450 nm) measured by customized ELISA in samples from healthy controls and patients with CKD. G1 indicates CKD patients with eGFR ≥90 and G2-5 with <90 mL/min/1.73m^2.

(B and C) ROC curve for distinguishing patients with decreased renal function (eGFR <60 (B), eGFR <90 (C)) from healthy controls by logistic regression.

(D) ROC curve for distinguishing patients with CKD having normal eGFR (≥90) from healthy controls by logistic regression.

(E) Box and beeswarm plot of the assay value of MGAM/MUC1 (the expression of MGAM divided by that of MUC1) in patients with CKD having each renal function and healthy controls in the discovery and validation cohorts.

(F) ROC curve for distinguishing patients with decreased renal function (eGFR <90) from healthy controls by logistic regression using combinations of MGAM/MUC1, urine creatinine (uCr), urine albumin (uAlb), and L-FABP.

(G) The change in eGFR in follow-up period in two groups (MGAM/MUC1 below 0.35 and the others). Boxes in boxplots indicate the 25th and 75th percentiles, and the horizontal lines inside the boxes indicate the median. Bars indicate the 10th and 90th percentiles. The data were compared using the two-tailed Mann–Whitney *U* test.

See also Figures S6–S8.

excretion of some vesicles by nephron loss has been shown previously (Blijdorp et al., 2022). Nephrectomy increased the proximal tubule markers NHE3, NaPi-IIa, and cubilin in uEVs, which is presumably caused by hypertrophy of the proximal tubules (Blijdorp et al., 2022). MGAM serves as an enzyme which functions in the final step of digestion of linear regions of starch to glucose (Nichols et al., 2003). Like other proximal tubule markers, increased expression of MGAM may be associated with compensatory response in proximal tubular cells.

The morphology of vesicles in whole urine (Blijdorp et al., 2021) or of uEVs was characterized in previous studies (Barreiro et al., 2020; Braun et al., 2020). The present study revealed that the variation in size in CKD was more significant than in healthy children (Figures 4D–4G). In this regard, the large vesicles increased in CKD were not supposed to be apoptotic bodies or autophagic extracellular vesicles because their markers (Annexin V or LC3B-PE, p62) (Jeppesen et al., 2019) were not detected in any of the samples. ARMMs were also excluded because their diameter is generally smaller than classic exosomes (Jeppesen et al., 2019). Therefore, from the aspect of size, the percentage of classical microvesicles, which is considered to be slightly larger in diameter than exosomes (Jeppesen et al., 2019), may be increasing in CKD. Another possibility is that they are exosomes enlarged because of dilution (Blijdorp et al., 2021). Dilution of urine is known to increase larger uEVs excreted (Blijdorp et al., 2021). We found that uEVs from samples with low urine creatinine tend to be larger (Figure S2). However, urine creatinine is affected by several factors in this cohort and cannot be used as a direct indicator of dilution. Fluid restriction in patients and controls will clarify how particle size fluctuates by dilution or concentration of urine. Together, it is preliminary to draw definitive conclusions about the mechanism of the difference in the size of uEVs in CKD.

The uEVs signature has significant potential as a non-invasive tool for diagnosing kidney diseases. Further large-scale prospective studies with a broader range of diseases and age groups with a more robust acquired component are warranted.

Limitation of the study

The present study is the first step in establishing the uEVs expression signature in childhood CKD, and some limitations should be acknowledged. First, it remains unclear whether the signature using Tim4-purified samples, which contained uEVs with various sizes and properties, are equally applicable to uEVs purified by other methods. Second, there is no definitive normalization strategy for quantitative proteome analysis for human body fluids (Erdbrügger et al., 2021; Théry et al., 2018). Previously proposed normalizing strategies include uEV number, a protein or RNA marker, total protein, RNA or lipid amount (Erdbrügger et al., 2021), or more recently, urine creatinine (Blijdorp et al., 2021). We applied total protein amount as normalizing variable because it can be obtained biochemically from uEVs without using different types of materials (i.e., whole urine) or experiments (i.e., NTA). Because it has been reported that there are a non-negligible amount of uEVs that do not express classical exosome markers such as CD9 or CD63 (Blijdorp et al., 2021), normalization using expression levels of one of these molecules might distort the results. Analysis using other standardization methods, such as urine creatinine (Blijdorp et al., 2021), is a subject for future study. Third, we could not clarify the correlation between the characteristics of uEVs and pathological changes. This is partly because most of the underlying diseases in this study, such as renal hypoplasia,

are not histologically diagnosed, and kidney biopsy is even contraindicated in these cases (Murugapoopathy and Gupta, 2020). Fourth, as high MGAM/MUC1 separates severe CKD patients, the baseline eGFR of the patients in MGAM/MUC1 > 0.35 group is decreased (Table S3), making it difficult to clarify whether the index detects factors related to prognosis beyond severity at study onset. Fifth, due to the small sample size of the discovery cohort, evaluation of AUC and a determination of optimal cut-off for sensitivity and specificity was only performed in the validation cohort. Finally, this study mainly included patients with congenital or inherited renal diseases involving the tubules in both cohorts, which is the major etiology of childhood CKD.

STAR★METHODS

Detailed methods are provided in the online version of this paper and include the following:

- KEY RESOURCES TABLE
- RESOURCE AVAILABILITY
  - Lead contact
  - Materials availability
  - Data and code availability
- EXPERIMENTAL MODEL AND SUBJECT DETAILS
  - Study design
  - Participants and samples
  - Study approval
- METHOD DETAILS
  - Tim4-affinity purification of uEVs
  - Nanoparticle tracking analysis
  - Transmission electron microscopy
  - Mass spectrometric analysis of uEVs
  - Mass spectrometry data processing
  - uEVs sandwich ELISA
  - Immunohistochemical analysis
  - Measurement of urine creatinine, albumin, liver-type fatty acid-binding protein (L-FABP) and urinary concentration of MUC1
- QUANTIFICATION AND STATISTICAL ANALYSIS

SUPPLEMENTAL INFORMATION

Supplemental information can be found online at https://doi.org/10.1016/j.isci.2022.105416.

ACKNOWLEDGMENTS

We thank S. Fukuda, and H. Kishita (The University of Tokyo) for their technical and instrumental support. This work is funded by Grants-in-Aid for Scientific Research from the Japan Society for the Promotion of Science (KAKENHI; grant number JP16K15523 to Y.H., and JP22K20847 to K.T.), by Japan Agency for Medical Research and Development (AMED; grant number JP20lm0203003 and JP21lm0203003, and JP22ym0126063h0001 to Y.H.), and by the University of Tokyo Gap Fund Program fifth period (to Y.H.).

AUTHOR CONTRIBUTIONS

K.T., K.U., and Y.H. conceived and designed the study. Y.H. coordinated the study. K.T., E.N., Y.K., S.K., K.M., M.H., J.H, Y.H., M.H., T.O., T.O., H.K., and N.F. enrolled patients in the study and collected urine samples and clinical information. K.T., K.U., E.N., T.N., and H.K. performed experiments. K.T. performed bioinformatics and statistical analyses and M.S. supervised these analyses. K.T., K.U., H.K., and Y.H. wrote and edited the manuscript. K.T. generated figures and tables. K.U., T.I., A.O., and Y.H. supervised the study. All authors participated in discussion and interpretation of the data and results.

DECLARATION OF INTERESTS

A patent application based on these results has been submitted by the University of Tokyo and Japanese Foundation for Cancer Research.

Received: May 30, 2022
Revised: September 7, 2022
Accepted: October 17, 2022
Published: November 8, 2022

REFERENCES

Akagi, T., Kato, K., Kobayashi, M., Kosaka, N., Ochiya, T., and Ichiki, T. (2015). On-chip immunoelectrophoresis of extracellular vesicles released from human breast cancer cells. PLoS One *10*, e0123603. https://doi.org/10.1371/journal.pone.0123603.

Akchurin, O.M., and Kaskel, F. (2015). Update on inflammation in chronic kidney disease. Blood Purif. *39*, 84–92. https://doi.org/10.1159/000368940.

Al-Bataineh, M.M., Sutton, T.A., and Hughey, R.P. (2017). Novel roles for mucin 1 in the kidney. Curr. Opin. Nephrol. Hypertens. *26*, 384–391. https://doi.org/10.1097/mnh.0000000000000350.

Awdishu, L., Tsunoda, S., Pearlman, M., Kokoy-Mondragon, C., Ghassemian, M., Naviaux, R.K., Patton, H.M., Mehta, R.L., Vijay, B., and RamachandraRao, S.P. (2019). Identification of maltase glucoamylase as a biomarker of acute kidney injury in patients with cirrhosis. Crit. Care Res. Pract. *2019*, 5912804. https://doi.org/10.1155/2019/5912804.

Barreiro, K., Dwivedi, O.P., Leparc, G., Rolser, M., Delic, D., Forsblom, C., Groop, P.H., Groop, L., Huber, T.B., Puhka, M., and Holthofer, H. (2020). Comparison of urinary extracellular vesicle isolation methods for transcriptomic biomarker research in diabetic kidney disease. J. Extracell. Vesicles *10*, e12038. https://doi.org/10.1002/jev2.12038.

Blijdorp, C.J., Hartjes, T.A., Wei, K.Y., van Heugten, M.H., Bovée, D.M., Budde, R.P.J., van de Wetering, J., Hoenderop, J.G.J., van Royen, M.E., Zietse, R., et al. (2022). Nephron mass determines the excretion rate of urinary extracellular vesicles. J. Extracell. Vesicles *11*, e12181. https://doi.org/10.1002/jev2.12181.

Blijdorp, C.J., Tutakhel, O.A.Z., Hartjes, T.A., van den Bosch, T.P.P., van Heugten, M.H., Rigalli, J.P., Willemsen, R., Musterd-Bhaggoe, U.M., Barros, E.R., Carles-Fontana, R., et al. (2021). Comparing approaches to normalize, quantify, and characterize urinary extracellular vesicles. J. Am. Soc. Nephrol. *32*, 1210–1226. https://doi.org/10.1681/asn.2020081142.

Braun, F., Rinschen, M., Buchner, D., Bohl, K., Plagmann, I., Bachurski, D., Richard Späth, M., Antczak, P., Göbel, H., Klein, C., et al. (2020). The proteomic landscape of small urinary extracellular vesicles during kidney transplantation. J. Extracell. Vesicles *10*, e12026. https://doi.org/10.1002/jev2.12026.

Dhondt, B., Lumen, N., De Wever, O., and Hendrix, A. (2020). Preparation of multi-omics grade extracellular vesicles by density-based fractionation of urine. STAR Protoc. *1*, 100073. https://doi.org/10.1016/j.xpro.2020.100073.

Dvela-Levitt, M., Kost-Alimova, M., Emani, M., Kohnert, E., Thompson, R., Sidhom, E.H., Rivadeneira, A., Sahakian, N., Roignot, J., Papagregoriou, G., et al. (2019). Small molecule targets TMED9 and promotes lysosomal degradation to reverse proteinopathy. Cell *178*, 521–535.e23. https://doi.org/10.1016/j.cell.2019.07.002.

Erdbrügger, U., Blijdorp, C.J., Bijnsdorp, I.V., Borràs, F.E., Burger, D., Bussolati, B., Byrd, J.B., Clayton, A., Dear, J.W., Falcón-Pérez, J.M., et al. (2021). Urinary extracellular vesicles: a position paper by the urine task force of the international society for extracellular vesicles. J. Extracell. Vesicles *10*, e12093. https://doi.org/10.1002/jev2.12093.

Erdbrügger, U., and Le, T.H. (2016). Extracellular vesicles in renal diseases: more than novel biomarkers? J. Am. Soc. Nephrol. *27*, 12–26. https://doi.org/10.1681/asn.2015010074.

Fathallah-Shaykh, S.A., Flynn, J.T., Pierce, C.B., Abraham, A.G., Blydt-Hansen, T.D., Massengill, S.F., Moxey-Mims, M.M., Warady, B.A., Furth, S.L., and Wong, C.S. (2015). Progression of pediatric CKD of nonglomerular origin in the CKiD cohort. Clin. J. Am. Soc. Nephrol. *10*, 571–577. https://doi.org/10.2215/cjn.07480714.

Fattah, H., Layton, A., and Vallon, V. (2019). How do kidneys adapt to a deficit or loss in nephron number? Physiology *34*, 189–197. https://doi.org/10.1152/physiol.00052.2018.

Gatto, L., and Lilley, K.S. (2012). MSnbase-an R/Bioconductor package for isobaric tagged mass spectrometry data visualization, processing and quantitation. Bioinformatics *28*, 288–289. https://doi.org/10.1093/bioinformatics/btr645.

Good, D.M., Zürbig, P., Argilés, A., Bauer, H.W., Behrens, G., Coon, J.J., Dakna, M., Decramer, S., Delles, C., Dominiczak, A.F., et al. (2010). Naturally occurring human urinary peptides for use in diagnosis of chronic kidney disease. Mol. Cell. Proteomics *9*, 2424–2437. https://doi.org/10.1074/mcp.M110.001917.

Harada, R., Hamasaki, Y., Okuda, Y., Hamada, R., and Ishikura, K. (2022). Epidemiology of pediatric chronic kidney disease/kidney failure: learning from registries and cohort studies. Pediatr. Nephrol. *37*, 1215–1229. https://doi.org/10.1007/s00467-021-05145-1.

Harambat, J., van Stralen, K.J., Kim, J.J., and Tizard, E.J. (2012). Epidemiology of chronic kidney disease in children. Pediatr. Nephrol. *27*, 363–373. https://doi.org/10.1007/s00467-011-1939-1.

Huber, W., Carey, V.J., Gentleman, R., Anders, S., Carlson, M., Carvalho, B.S., Bravo, H.C., Davis, S., Gatto, L., Girke, T., et al. (2015). Orchestrating high-throughput genomic analysis with Bioconductor. Nat. Methods *12*, 115–121. https://doi.org/10.1038/nmeth.3252.

Huber, W., von Heydebreck, A., Sültmann, H., Poustka, A., and Vingron, M. (2002). Variance stabilization applied to microarray data calibration and to the quantification of differential expression. Bioinformatics *18* (*Suppl 1*), S96–S104. https://doi.org/10.1093/bioinformatics/18.suppl_1.s96.

Ingelfinger, J.R., Kalantar-Zadeh, K., and Schaefer, F.; World Kidney Day Steering Committee (2016). Averting the legacy of kidney disease–focus on childhood. Kidney Int. *89*, 512–518. https://doi.org/10.1016/j.kint.2015.10.014.

Jeppesen, D.K., Fenix, A.M., Franklin, J.L., Higginbotham, J.N., Zhang, Q., Zimmerman, L.J., Liebler, D.C., Ping, J., Liu, Q., Evans, R., et al. (2019). Reassessment of exosome composition. Cell *177*, 428–445.e18. https://doi.org/10.1016/j.cell.2019.02.029.

Kirby, A., Gnirke, A., Jaffe, D.B., Barešová, V., Pochet, N., Blumenstiel, B., Ye, C., Aird, D., Stevens, C., Robinson, J.T., et al. (2013). Mutations causing medullary cystic kidney disease type 1 lie in a large VNTR in MUC1 missed by massively parallel sequencing. Nat. Genet. *45*, 299–303. https://doi.org/10.1038/ng.2543.

Levey, A.S., Eckardt, K.U., Tsukamoto, Y., Levin, A., Coresh, J., Rossert, J., De Zeeuw, D., Hostetter, T.H., Lameire, N., and Eknoyan, G. (2005). Definition and classification of chronic kidney disease: a position statement from Kidney Disease: Improving Global Outcomes (KDIGO). Kidney Int. *67*, 2089–2100. https://doi.org/10.1111/j.1523-1755.2005.00365.x.

Martens, M., Ammar, A., Riutta, A., Waagmeester, A., Slenter, D.N., Hanspers, K., A Miller, R., Digles, D., Lopes, E.N., Ehrhart, F., et al. (2021). WikiPathways: connecting communities. Nucleic Acids Res. *49*, D613–D621. https://doi.org/10.1093/nar/gkaa1024.

Merchant, M.L., Rood, I.M., Deegens, J.K.J., and Klein, J.B. (2017). Isolation and characterization of urinary extracellular vesicles: implications for biomarker discovery. Nat. Rev. Nephrol. *13*, 731–749. https://doi.org/10.1038/nrneph.2017.148.

Murugapoopathy, V., and Gupta, I.R. (2020). A primer on congenital anomalies of the kidneys and urinary tracts (CAKUT). Clin. J. Am. Soc. Nephrol. *15*, 723–731. https://doi.org/10.2215/cjn.12581019.

Nakai, W., Yoshida, T., Diez, D., Miyatake, Y., Nishibu, T., Imawaka, N., Naruse, K., Sadamura, Y., and Hanayama, R. (2016). A novel affinity-based method for the isolation of highly purified extracellular vesicles. Sci. Rep. *6*, 33935. https://doi.org/10.1038/srep33935.

Nichols, B.L., Avery, S., Sen, P., Swallow, D.M., Hahn, D., and Sterchi, E. (2003). The maltase-glucoamylase gene: common ancestry to sucrase-isomaltase with complementary starch digestion activities. Proc. Natl. Acad. Sci. USA

100, 1432–1437. https://doi.org/10.1073/pnas.0237170100.

Nie, M., Bal, M.S., Yang, Z., Liu, J., Rivera, C., Wenzel, A., Beck, B.B., Sakhaee, K., Marciano, D.K., and Wolf, M.T.F. (2016). Mucin-1 increases renal TRPV5 activity in vitro, and urinary level associates with calcium nephrolithiasis in patients. J. Am. Soc. Nephrol. *27*, 3447–3458. https://doi.org/10.1681/asn.2015101100.

Pisitkun, T., Shen, R.F., and Knepper, M.A. (2004). Identification and proteomic profiling of exosomes in human urine. Proc. Natl. Acad. Sci. USA *101*, 13368–13373. https://doi.org/10.1073/pnas.0403453101.

Pontillo, C., Jacobs, L., Staessen, J.A., Schanstra, J.P., Rossing, P., Heerspink, H.J.L., Siwy, J., Mullen, W., Vlahou, A., Mischak, H., et al. (2017). A urinary proteome-based classifier for the early detection of decline in glomerular filtration. Nephrol. Dial. Transplant. *32*, 1510–1516. https://doi.org/10.1093/ndt/gfw239.

Ransick, A., Lindström, N.O., Liu, J., Zhu, Q., Guo, J.J., Alvarado, G.F., Kim, A.D., Black, H.G., Kim, J., and McMahon, A.P. (2019). Single-cell profiling reveals sex, lineage, and regional diversity in the mouse kidney. Dev. Cell *51*, 399–413.e7. https://doi.org/10.1016/j.devcel.2019.10.005.

Ritchie, M.E., Phipson, B., Wu, D., Hu, Y., Law, C.W., Shi, W., and Smyth, G.K. (2015). Limma powers differential expression analyses for RNA-sequencing and microarray studies. Nucleic Acids Res. *43*, e47. https://doi.org/10.1093/nar/gkv007.

Rosenbaum, D.M., Korngold, E., and Teele, R.L. (1984). Sonographic assessment of renal length in normal children. AJR Am. J. Roentgenol. *142*, 467–469. https://doi.org/10.2214/ajr.142.3.467.

Ruiz-Ortega, M., Rayego-Mateos, S., Lamas, S., Ortiz, A., and Rodrigues-Diez, R.R. (2020). Targeting the progression of chronic kidney disease. Nat. Rev. Nephrol. *16*, 269–288. https://doi.org/10.1038/s41581-019-0248-y.

Salih, M., Demmers, J.A., Bezstarosti, K., Leonhard, W.N., Losekoot, M., van Kooten, C., Gansevoort, R.T., Peters, D.J.M., Zietse, R., and Hoorn, E.J.; DIPAK Consortium (2016). Proteomics of urinary vesicles links plakins and complement to polycystic kidney disease. J. Am. Soc. Nephrol. *27*, 3079–3092. https://doi.org/10.1681/asn.2015090994.

Sandilands, E.A., Dhaun, N., Dear, J.W., and Webb, D.J. (2013). Measurement of renal function in patients with chronic kidney disease. Br. J. Clin. Pharmacol. *76*, 504–515. https://doi.org/10.1111/bcp.12198.

Schnaper, H.W. (2014). Remnant nephron physiology and the progression of chronic kidney disease. Pediatr. Nephrol. *29*, 193–202. https://doi.org/10.1007/s00467-013-2494-8.

Schwartz, G.J., Muñoz, A., Schneider, M.F., Mak, R.H., Kaskel, F., Warady, B.A., and Furth, S.L. (2009). New equations to estimate GFR in children with CKD. J. Am. Soc. Nephrol. *20*, 629–637. https://doi.org/10.1681/asn.2008030287.

Smyth, G.K. (2004). Linear models and empirical bayes methods for assessing differential expression in microarray experiments. Stat. Appl. Genet. Mol. Biol. *3*. Article3. https://doi.org/10.2202/1544-6115.1027.

Stern-Zimmer, M., Calderon-Margalit, R., Skorecki, K., and Vivante, A. (2020). Childhood risk factors for adulthood chronic kidney disease. Pediatr. Nephrol. *36*, 1387–1396. https://doi.org/10.1007/s00467-020-04611-6.

Théry, C., Witwer, K.W., Aikawa, E., Alcaraz, M.J., Anderson, J.D., Andriantsitohaina, R., Antoniou, A., Arab, T., Archer, F., Atkin-Smith, G.K., et al. (2018). Minimal information for studies of extracellular vesicles 2018 (MISEV2018): a position statement of the International Society for Extracellular Vesicles and update of the MISEV2014 guidelines. J. Extracell. Vesicles *7*, 1535750. https://doi.org/10.1080/20013078.2018.1535750.

Tkach, M., and Théry, C. (2016). Communication by extracellular vesicles: where we are and where we need to go. Cell *164*, 1226–1232. https://doi.org/10.1016/j.cell.2016.01.043.

Udagawa, T., Harita, Y., Miura, K., Mitsui, J., Ode, K.L., Morishita, S., Urae, S., Kanda, S., Kajiho, Y., Tsurumi, H., et al. (2018). Amnionless-mediated glycosylation is crucial for cell surface targeting of cubilin in renal and intestinal cells. Sci. Rep. *8*, 2351. https://doi.org/10.1038/s41598-018-20731-4.

Uemura, O., Ishikura, K., Gotoh, Y., and Honda, M. (2018). Creatinine-based estimated glomerular filtration rate for children younger than 2 years. Clin. Exp. Nephrol. *22*, 483–484. https://doi.org/10.1007/s10157-017-1460-3.

Uemura, O., Nagai, T., Ishikura, K., Ito, S., Hataya, H., Gotoh, Y., Fujita, N., Akioka, Y., Kaneko, T., and Honda, M. (2014). Creatinine-based equation to estimate the glomerular filtration rate in Japanese children and adolescents with chronic kidney disease. Clin. Exp. Nephrol. *18*, 626–633. https://doi.org/10.1007/s10157-013-0856-y.

van Niel, G., D'Angelo, G., and Raposo, G. (2018). Shedding light on the cell biology of extracellular vesicles. Nat. Rev. Mol. Cell Biol. *19*, 213–228. https://doi.org/10.1038/nrm.2017.125.

Watson, D., Yang, J.Y.C., Sarwal, R.D., Sigdel, T.K., Liberto, J.M., Damm, I., Louie, V., Sigdel, S., Livingstone, D., Soh, K., et al. (2019). A novel multi-biomarker assay for non-invasive quantitative monitoring of kidney injury. J. Clin. Med. *8*, E499. https://doi.org/10.3390/jcm8040499.

Webster, A.C., Nagler, E.V., Morton, R.L., and Masson, P. (2017). Chronic kidney disease. Lancet *389*, 1238–1252. https://doi.org/10.1016/s0140-6736(16)32064-5.

ESCAPE Trial Group, Wühl, E., Trivelli, A., Picca, S., Litwin, M., Peco-Antic, A., Zurowska, A., Testa, S., Jankauskiene, A., Emre, S., Caldas-Afonso, A., et al. (2009). Strict blood-pressure control and progression of renal failure in children. N. Engl. J. Med. *361*, 1639–1650. https://doi.org/10.1056/NEJMoa0902066.

Zhang, X., Smits, A.H., van Tilburg, G.B., Ovaa, H., Huber, W., and Vermeulen, M. (2018). Proteome-wide identification of ubiquitin interactions using UbIA-MS. Nat. Protoc. *13*, 530–550. https://doi.org/10.1038/nprot.2017.147.

Zhang, Z.Y., Ravassa, S., Pejchinovski, M., Yang, W.Y., Zürbig, P., López, B., Wei, F.F., Thijs, L., Jacobs, L., González, A., et al. (2017). A urinary fragment of mucin-1 subunit α is a novel biomarker associated with renal dysfunction in the general population. Kidney Int. Rep. *2*, 811–820. https://doi.org/10.1016/j.ekir.2017.03.012.

STAR★METHODS

KEY RESOURCES TABLE

REAGENT or RESOURCE	SOURCE	IDENTIFIER
Antibodies		
Rabbit polyclonal anti-MGAM	Proteintech	Cat# 22195-1-AP, RRID:AB_2879023
Mouse monoclonal anti-MUC1	Santa Cruz Biotechnology	Cat# sc-7313, RRID:AB_626983
Mouse monoclonal anti-CD9 (clone 12A12)	Shionogi & Co	SHI-EXO-M01
Mouse monoclonal anti-poliovirus receptor (PVR)	Proteintech	Cat# 66913-1-Ig, RRID:AB_2882240
Mouse monoclonal anti-PKD2	Abnova	Cat# H00005311-M01 RRID:AB_606781
Mouse monoclonal anti-CD133 (PROM1)	Proteintech	Cat# 66666-1-Ig, RRID:AB_2801586
Rabbit monoclonal anti-CD90/Thy1	Abcam	Cat# ab92574, RRID:AB_10563647
Mouse monoclonal anti-GGT1	Santa Cruz Biotechnology	Cat# sc-166908, RRID:AB_10608594
Mouse monoclonal anti-THP	Santa Cruz Biotechnology	Cat# sc-271022, RRID:AB_10610634
Rabbit polyclonal anti-PGK1	Proteintech	Cat# 17811-1-AP, RRID:AB_2161218
Rabbit polyclonal anti-Cytokeratin14(KRT14)	Proteintech	Cat# 10143-1-AP, RRID:AB_2134831
Rabbit polyclonal anti-AnnexinA11(ANXA11)	Proteintech	Cat# 10479-2-AP, RRID:AB_2057171
Biological samples		
Human adult normal kidney tissue	BioChain	Cat# T2234142
Critical commercial assays		
Biotin labeling kit-NH2	Dojindo Molecular Technologies	LK-03
PS Capture Exosome ELISA Kit	Wako Pure Chemical Industries	Cat# 298-80601
MagCapture Exosome Isolation Kit PS	Wako Pure Chemical Industries	Cat# 293-77601
Creatinine Companion kit	Exocell	Cat# 1012
Albuwell Hu	Exocell	Cat# 1004
High Sensitivity Human L-FABP ELISA Kit	CMIC CoLtd	Cat# 006
Human MUCIN 1 (CA15-3) ELISA Kit	Thermo Fisher Scientific	Cat# EHMUC1
Deposited data		
Kidney cell explorer	(Ransick et al., 2019)	https://cello.shinyapps.io/kidneycellexplorer/
Software and algorithms		
R software version 3.5.1	https://www.R-project.org/	N/A
GraphPad Prism software version 9.2.0	https://www.graphpad.com/scientific-software/prism	N/A
DEP	(Zhang et al., 2018)	https://bioconductor.org/packages/release/bioc/html/DEP.html
g:Profiler	https://biit.cs.ut.ee/gprofiler/gost	N/A
Other		
iMark™ Microplate Absorbance Reader	Bio-Rad Laboratories	Cat# 168-1130J5
NanoSight LM10 system	NanoSight Ltd	N/A
Orbitrap Fusion Lumos mass spectrometer	Thermo Fisher Scientific	Cat# IQLAAEGAAPFADBMBHQ
UltiMate 3000 RSLC nano-flow HPLC	Thermo Fisher Scientific	Cat# ULTIM3000RSLCNANO
Transmission electron microscopy	Hitachi Ltd	Hitachi H-7000
All-in-One Fluorescence Microscope	KEYENCE Japan	BZ-X810

RESOURCE AVAILABILITY

Lead contact

Further information and requests for resources and reagents should be directed to and will be fulfilled by the lead contact, Yutaka Harita (haritay-ped@h.u-tokyo.ac.jp).

Materials availability

This study did not generate new unique reagents.

Data and code availability

This paper does not report original code.

Data reported in this paper will be shared by the lead contact upon request.

Any additional information required to reanalyze the data reported in this paper is available from the lead contact upon request.

EXPERIMENTAL MODEL AND SUBJECT DETAILS

Study design

As a model of fewer nephrons, we focused on differences in molecular expression in uEVs between healthy controls and patients with renal hypoplasia. Molecules differentially expressed in the two groups were used for the subsequent analysis integrating other CKD patients (Discovery cohort). The physical characteristics of uEVs in CKD were analyzed by nanoparticle tracking analysis (NTA). Next, we established a system to quantify candidate biomarkers' protein content in uEVs using enzyme-linked immunosorbent assay (ELISA). Finally, we evaluated the diagnostic performance of the system using newly collected urine samples from healthy controls and CKD patients (Validation cohort).

Participants and samples

Subjects in the discovery cohort were recruited from 5 child hospitals or centers in Japan from June 2016 to June 2018. Healthy controls and patients with CKD in the validation cohort were recruited from 8 centers in Japan from June 2019 to June 2021. All cases were comprehensively diagnosed based on symptoms, blood tests, urinalysis, kidney biopsy findings, ultrasound results, imaging tests, such as CT, MRI, voiding cystourethrography, and scintigraphy, when available. Clinical data were registered in an electronic database. The estimated glomerular filtration rate (eGFR) was calculated using the polynomial eGFR formula (Uemura et al., 2014) for participants older than 2 years, the polynomial eGFR formula multiplied by a factor (Uemura et al., 2018) for participants older than 3 months and younger than 2 years, and the Schwartz formula (Schwartz et al., 2009) for participants younger than 3 months. The classification of patients with CKD by eGFR was performed according to the Kidney Disease: Improving Global Outcomes guidelines for chronic kidney disease stage classification (Levey et al., 2005). Details about patients' characteristics in each cohort are given in Tables 1 and 2. Written informed consent was obtained from all enrolled patients or their parents. After urine samples were collected, they were frozen and transferred to our laboratory, where they were thawed and aliquoted 200 μL in each case and frozen at −80°C. The samples were thawed before the experiment.

Study approval

This study was approved by the ethics committee of the University of Tokyo (#11106-(3)).

METHOD DETAILS

Tim4-affinity purification of uEVs

Purification of EVs from urine with Tim4-affinity beads (Nakai et al., 2016) was performed using the MagCapture Exosome Isolation Kit PS (Cat# 293-77601 FUJIFILM Wako Pure Chemical Corporation, Osaka, Japan) following the manufacturer's protocol. Urine samples were centrifuged at 1,200 × *g* for 20minat 4°C to remove cell debris and urine salts and then centrifuged at 10,000 × *g* for 30 min at 4°C to remove the large EVs such as apoptotic bodies. Streptavidin magnetic beads, bound with biotinylated Tim4, were added to 1 mL of the supernatant supplemented with 2 mM $CaCl_2$, and the mixture was rotated for 1hat 20–25°C. The beads were washed three times with 1 mL washing buffer (20 mM Tris-HCl, pH 7.4,

150 mM NaCl, 0.0005% Tween 20, 2 mM $CaCl_2$), and the bound uEVs were eluted with an elution buffer (20 mM Tris-HCl, pH 7.4, 150 mM NaCl, 2 mM EDTA).

Nanoparticle tracking analysis

Purified uEVs were analyzed by nanoparticle tracking using a NanoSight LM10 system (NanoSight Ltd., Amesbury, UK) configured with a 405 nm laser and a high-sensitivity sCMOS camera (OrcaFlash2.8, Hamamatsu C11440, NanoSight Ltd.). The measurements were performed as previously described (Akagi et al., 2015). Prior to analysis, sample aliquots were diluted 20- to 40-fold in particle-free 4-(2-hydroxyethyl)-1-piperazineethanesulfonic acid (HEPES, Thermo Fisher Scientific, MA, USA) buffer to achieve optimal concentration for analysis; a diluted sample (1 mL) was used for each analysis. Light scattering of individual particles in solution was digitally recorded, and particle trajectory and displacement were automatically analyzed using an image analysis tracking software. The particle size distribution was determined from the observed Brownian motion of individual particles according to the Stokes–Einstein relationship.

Transmission electron microscopy

Purified uEVs samples were placed on carbon-coated holey-film grids for 5minat 4°C. Following sample adsorption, grids were quickly and gently blotted on filter paper and immediately floated for 5 min on 1 mL of 1% uranyl acetate at 4°C and dried on filter paper. Imaging was performed on electron microscopy (Hitachi H-7000, Tokyo, Japan). Micrographs were captured with a 2k x 2k CCD camera.

Mass spectrometric analysis of uEVs

According to the manufacturer's instruction, EVs were purified from 1 mL of urine samples using MagCapture Exosome Isolation Kit PS (FUJIFILM Wako Pure Chemical Corporation), except for elution with 30 μL of 1 × Laemmli's sample buffer. After reduction with 10 mM TCEP at 100°C for 10 min and alkylation with 50 mM iodoacetamide at ambient temperature for 45 min, protein samples were subjected to SDS-PAGE. The electrophoresis was stopped at the migration distance of 2 mm from the top edge of the separation gel. After CBB-staining, protein bands were excised, destained, and cut finely prior to in-gel digestion with Trypsin/Lys-C Mix (Promega) at 37°C for 12 hours. The resulting peptides were extracted from gel fragments and analyzed with Orbitrap Fusion Lumos mass spectrometer (Thermo Fisher Scientific) combined with UltiMate 3000 RSLC nano-flow HPLC (Thermo Fisher Scientific). Peptides were enriched with μ-Precolumn (0.3 mm i.d. × 5 mm, 5 μm, Thermo Fisher Scientific) and separated on AURORA column (0.075 mm i.d. × 250 mm, 1.6 μm, Ion Opticks Pty Ltd, Australia) using the two-step gradient; 2–40% acetonitrile for 110 min, followed by 40-95% acetonitrile for 5 min in the presence of 0.1% formic acid. The analytical parameters of Orbitrap Fusion Lumos were set as follows; Resolution of full scans = 50,000, Scan range (m/z) = 350-1500, Maximum injection time of full scans = 50 msec, AGC target of full scans = 4×10^5, Dynamic exclusion duration = 30 sec, Cycle time of data-dependent MS/MS acquisition = 2 sec, Activation-type = HCD, Detector of MS/MS = Ion trap, Maximum injection time of MS/MS = 35 msec, AGC target of MS/MS = 1×10^4. The MS/MS spectra were searched against the *Homo sapiens* protein sequence database (20,366 entries) in SwissProt using Proteome Discoverer 2.4 software (Thermo Fisher Scientific), in which peptide identification filters were set at "false discovery rate <1%". Label-free relative quantification analysis for proteins was performed with the default parameters of Minora Feature Detector node, Feature Mapper node, and Precursor Ions Quantifier node in Proteome Discoverer 2.4 software.

Mass spectrometry data processing

The LC-MS/MS dataset was loaded into the R package DEP (Zhang et al., 2018), which provides an integrated analysis workflow for differential protein expression or differential enrichment analysis. This package is integrated within the Bioconductor project (Huber et al., 2015) and includes functionalities to filter and normalize data, perform differential enrichment testing, and visualize the results. In the analysis, the data are filtered for proteins with many missing values, after which variance-stabilizing transformation using vsn (Huber et al., 2002) and data imputation using the methods from MSnbase (Gatto and Lilley, 2012) are applied. Subsequently, differential enrichment analysis is performed by applying empirical Bayesian statistics to protein-wise linear models using limma (Ritchie et al., 2015; Smyth, 2004). In addition, the results can be explored using different visualizations, including a volcano plot (an adjusted p value <0.5 and Log2 fold change >2.5) and MDS analysis. MDS analysis with Spearman's rank correlation and k-means was carried out using the *cmdscale* package in R. Heatmap was plotted using the *pheatmap* R package (version 1.0.12). We used Euclidean as the popular clustering distance and method implemented in the *dist* and

hclust functions in R. The gene ontology (GO) terms and KEGG/Wiki pathway terms enriched in the predicted target genes were determined using g:Profiler bioinformatics.

uEVs sandwich ELISA

Before ELISA, thawed urine samples were centrifuged at 1,200 × *g* for 20minat 4°C to remove cell debris and urine salts. ELISA was performed using the PS Capture Exosome ELISA Kit (Cat# 298-80601 FUJIFILM Wako Pure Chemical Corporation, Osaka, Japan) according to the manufacturer's instructions. Absorbance at 450 nm was measured using the iMark microplate Absorbance Spectrophotometer (Bio-Rad). Antibodies used as capture reagents were as follows: anti-CD63 antibody contained in the abovementioned kit, and mouse monoclonal anti-CD9 antibody (clone12A12, Shionogi, Osaka, Japan), rabbit polyclonal anti-MGAM antibody (Cat# 22195-1-AP, Proteintech, Chicago, IL, USA), mouse monoclonal anti-MUC1 antibody (Cat# sc-7313, Santa Cruz, Dallas, TX, USA), mouse monoclonal anti-Poliovirus receptor (PVR) antibody (Cat# 66913-1-Ig, Proteintech), mouse monoclonal anti-PKD2 antibody (Cat# H00005311-M01, Abnova, Taipei, Taiwan), mouse monoclonal anti-CD133 (PROM1) antibody (Cat# 66666-1-Ig, Proteintech), and rabbit monoclonal anti-CD90/Thy1 antibody (Cat# ab92574, Abcam, Cambridge, UK). For the latter three antibodies, biotin was conjugated to them using the biotin labeling kit-NH2 (Dojindo, Kumamoto, Japan), according to the manufacturer's instructions.

Immunohistochemical analysis

Immunohistochemical analyses were performed as previously described (Udagawa et al., 2018). Paraffin-embedded human adult normal kidney tissue (Cat# T2234142, Biochain, Newark, CA, USA) were deparaffinized in xylene and rehydrated through a series of graded alcohols in H_2O, followed by heat-induced epitope retrieval by incubating in a target retrieval solution (S1699; Dako, Carpinteria, CA, USA) for 20minat 121°C. Sections were cooled to room temperature and incubated with primary antibodies, followed by incubation with Alexa Fluor conjugated secondary antibodies (Invitrogen). Mouse monoclonal anti-GGT1 antibody (Cat# sc-166908, Santa Cruz), mouse monoclonal anti-THP (UMOD) antibody (Cat# sc-271022, Santa Cruz), rabbit polyclonal anti-PGK1 antibody (Cat# 17811-1-AP, Proteintech), rabbit polyclonal anti-KRT14 antibody (Cat# 10143-1-AP, Proteintech), rabbit polyclonal anti-ANXA11 antibody (Cat# 10479-2-AP, Proteintech) and above mentioned anti-CD9 antibody, anti-MGAM antibody, and anti-MUC1 antibody were used as primary antibodies. Confocal fluorescent images were obtained using a KEYENCE Japan BZ-X810 microscope.

Measurement of urine creatinine, albumin, liver-type fatty acid-binding protein (L-FABP) and urinary concentration of MUC1

The urine creatinine, albumin, L-FABP or urinary concentration of MUC1 were measured using commercially available enzyme-linked immunosorbent assay kits (The Creatinine Companion kit and Albuwell Hu; Exocell, Philadelphia, PA; High Sensitivity Human L-FABP ELISA Kit; CMIC CoLtd, Tokyo, Japan; Human MUCIN 1 (CA15-3) ELISA Kit; Thermo Fisher Scientific), according to the manufacturer's instructions.

QUANTIFICATION AND STATISTICAL ANALYSIS

Data are expressed as the mean ± SD. Groups were compared using two-tailed Mann-Whitney test or Welch's *t* test according to Gaussian distribution assessed by Shapiro-Wilk test. For correlation studies, a Pearson coefficient was reported as R (confidence interval). p value was considered significant when $p < 0.05$. Boxes in boxplots indicate the 25th and 75th percentiles, and the horizontal lines inside the boxes indicate the median. Bars indicate the 10th and 90th percentiles. Statistical analyses were performed using GraphPad Prism software version 9.2.0 or the R software version 3.5.1 (https://www.R-project.org/). DEP package (version 1.14.0) was used for differential analyses between two conditions. Pwr.t.test from the pwr package (version 1.3-0) was used to calculate sample size. ROC curves in logistic regression were adopted to determine the diagnostic metrics of biomarkers. Optimal cutoff points were selected using the maximum Youden's index to determine disease diagnostic sensitivity, specificity, and accuracy. For each experiment, the samples were blinded for the person in charge of conducting the experiment and data processing. All data excluding outliers are shown, and all experiments were performed in at least triplicate. Technical replicates were not considered as independent samples; thus, multiple technical replicates of the same one biological sample were counted as $N = 1$.